

Numerical identification of Preisach distribution function including temperature effects

LEILA CHELGHOU 

*University Hadj Lakhdar Batna 1
Batna, Algeria*

e-mail: leila.chelghoum@univ-batna.dz

(Received: 17.06.2021, revised: 29.10.2021)

Abstract: Magnetic hysteresis occurs in most electrical engineering devices once soft ferromagnetic materials are exposed to relatively high temperatures. According to several scientific studies, magnetic properties are strongly influenced by temperature. The development of models that can accurately describe the thermal effect on ferromagnetic materials is still an issue that inspires researchers. In this paper, the effect of temperature on magnetic hysteresis for ferromagnetic materials is investigated using a self-developed numerical method based on the Preisach distribution function identification. It employs a parameter depending on both temperature and the Curie temperature. This approach is of the macroscopic phenomenological type, where the variation of the magnetization (in direct connection with the Preisach triangle) is related to the observed macroscopic hysteretic behavior. The isotropic character of the material medium is predominant. The technique relies on a few experimental data extracted from the first magnetization curve provided by metallurgists. The ultimate goal is to provide a simple and robust magnetic behavior modeling tool for designers of electrical devices. Temperature is introduced at the stage of identifying the distribution function of the Preisach model. This method is validated by the agreement between the experimental data and the simulation results. The developed method is very accurate and efficient in modeling the hysteresis of ferromagnetic materials in engineering particularly for systems with ferromagnetic components and electromagnetic-thermal coupling.

Key words: magnetic hysteresis, Preisach distribution function, Preisach model, soft ferromagnetic materials, temperature effect



1. Introduction

Several scientific studies have showcased the very close dependence of the properties of ferromagnetic materials on temperature. In order to predict their behavior once integrated into electrical devices, the development of temperature-dependent hysteresis models remains an important issue for researchers. The two well-known models Jiles–Atherthon [1–3] and Preisach [4–15] have been widely used in the analytical modeling of magnetic hysteresis and in the calculation of magnetic losses in electromagnetic systems [6]. In the analytical modeling of hysteresis using the Preisach model, most authors have determined a shape for the Preisach distribution function with which they have associated one or more temperature dependent parameters [8, 9, 16]. The influence of temperature has frequently been disregarded or eliminated in the numerical approach employing the Preisach model. Among the few contributions that have attempted to take temperature into account in the hysteresis models, we cite:

The authors of [5] have combined a Preisach operator with a temperature-dependent weight function. Its parameters have been determined by taking into account the properties of hysteresis curves of ferromagnetic samples. In a more recent work [7], the parameters of the Vector Play static hysteresis model have been modified so as to predict the thermal behavior. In [8, 9] and [16], a critical exponent has been introduced both in the coercive field and in the saturation magnetization, to simulate hysteresis loops at different temperatures using the Preisach model. In [14], the authors have measured the major hysteresis loops of soft ferrite core samples at different temperatures and have concluded that the saturation points are temperature-dependent in a nonlinear manner. Furthermore, the results have revealed that in the operating temperature range, typically 20°C–100°C, the variation can be considered linear with an extremely low error. They have proposed a new method based on this approximation to obtain limiting hysteresis loops. The authors of [15] have developed a model based on two temperature-dependent parameters: a behavioral coefficient and a static function which have determined at a temperature value that corresponds to minimum loss. To describe the influence of temperature on the magnetic characteristics of ferrite samples, each parameter has been studied separately.

This work is distinguished by the introduction of the temperature effect at the stage of the distribution function identification which is the essence of the Preisach model formulation [4, 10, 13]. It should be noted that a self-developed numerical method of Preisach distribution function identification [12] is used.

2. Classical static Preisach model

According to the Preisach model [10], the magnetic field $H(t)$ and magnetization $M(t)$ are related by:

$$M(t) = \iint_{\alpha \geq \beta} v(\alpha, \beta), \quad R_{\alpha, \beta}[H(t)] d\alpha d\beta, \quad (1)$$

where $v(\alpha, \beta)$ is the Preisach density function:

$$v(\alpha, \beta) \geq 0. \quad (2)$$

At any instant t (Fig. 1), e.g. (1) can be written [10, 12]:

$$M(t) = \iint_{S^+(t)} \nu(\alpha, \beta) d\alpha d\beta - \iint_{S^-(t)} \nu(\alpha, \beta) d\alpha d\beta. \quad (3)$$

The identification of the distribution function is a crucial step in modelling hysteresis with the Preisach model. In the specialized literature, there are two approaches to identify the Preisach distribution function: the analytical approach and the numerical one. Briefly, we will explain the link between the (H, M) curve and the Preisach triangle [10, 12, 13].

Increasing the excitation from $(-H_s)$ to (H_1) , we obtain the part of the magnetization curve that corresponds to $(M(-H_s), M(H_1))$ with $M(H_1) = M_{\alpha_1}$ (Fig. 1(a)). When the excitation is decreased to the value $(H_2 = \beta_1)$, we obtain the part of the magnetization curve corresponding to the value $(M_{\alpha_1\beta_1})$ (Fig. 1(b)). The triangle cell $T(\alpha_1, \beta_1)$ appears (Fig. 1(b)), it corresponds to the variation in the magnetization between the two different states $(\alpha_1 = H_1, M_{\alpha_1})$ and $(\beta_1 = H_2, M_{\alpha_1\beta_1})$ and given by [10, 12]:

$$\Delta M = (M_{\alpha_1} - M_{\alpha_1\beta_1}) = 2 \iint_{T(\alpha_1, \beta_1)} \nu(\alpha, \beta) d\alpha d\beta. \quad (4)$$

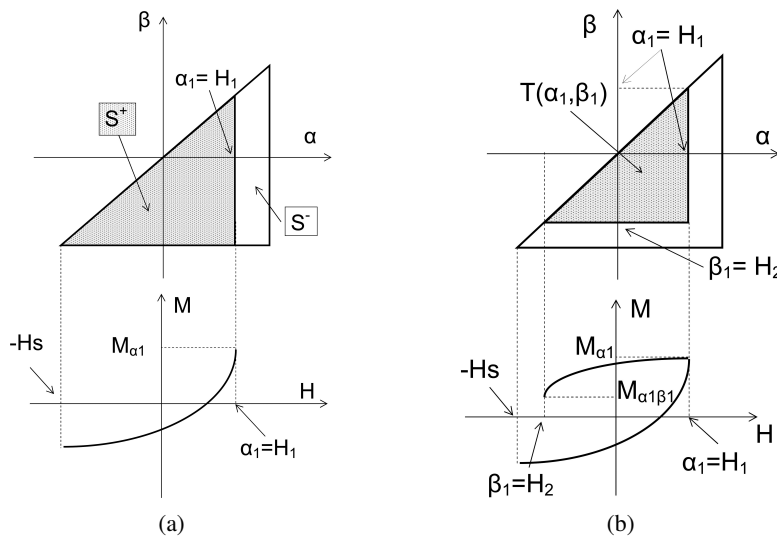


Fig. 1. An increase and a decrease of the magnetic field in the (H, M) -plane as well as their geometrical representations in the Preisach plane (respectively, Fig. 1(a) and Fig. 1(b)), the variation of the magnetization is represented by the triangle $T(\alpha_1, \beta_1)$, Fig. 1(b)

Equation (4) constitutes a bijective relationship between the discretization of the Preisach triangle (the right-hand side of e.g. (4)) and magnetization variation (the left-hand side of e.g. (4)). Also, it should be noted that each cell of the discretized Preisach triangle provides information about numerical value of the Preisach density function [12].

3. Numerical Preisach density function identification including temperature effects

Considering the non-linearity of the magnetic hysteresis cycle and its established dependence on temperature [4, 9, 10]. When T increases to the Curie temperature T_c , M_s decreases to zero and the ferromagnetic material changes to paramagnetic [8]. In publications dealing with the analytical modeling of the magnetic hysteresis using the Preisach model, authors selected a shape for the distribution function and also a temperature-dependent parameter which was a continuous function of temperature T [3, 8, 9] and [16]. In this study and in order to determine an optimal temperature-dependent parameter, several numerical simulations with different shapes of this parameter were carried out. Finally, we opted for two of them noted $\beta(T)$ and $\theta(T)$, taken respectively from [8] and [16], whose results are in agreement with available experimental data (Fig. 2).

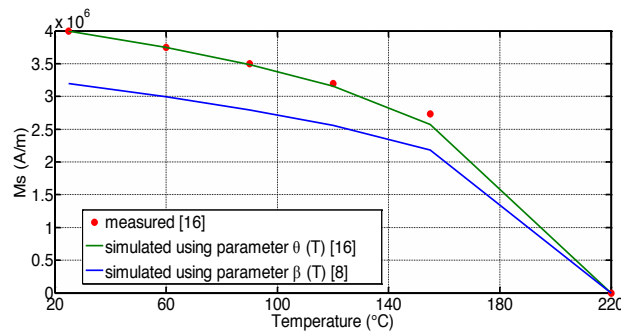


Fig. 2. Effects of the two temperature-dependent parameters $\beta(T)$ and $\theta(T)$ [8, 16] on the saturation magnetization (M_s) compared to experimental data [16]

Figure 2 shows a comparison of $M_s(T)$ given by the two temperature-dependent parameters $\beta(T)$ and $\theta(T)$ for different temperatures with experimental data [16]. It appears that parameter $\theta(T)$ gives better results. This explains our choice, the parameter $\theta(T)$ given by:

$$\theta(T) = \left(1 - \exp\left(\frac{(T - T_c)}{\tau}\right) \right). \quad (5)$$

First, we will recall the main steps of the numerical identification technique. In the identification process, the following assumptions were considered:

- i – Uniformity of the density function per cell of the discretized Preisach triangle.
- ii – Symmetry of the density function with respect to the line ($\alpha = -\beta$) in the Preisach triangle.

For the development of our temperature-dependent numerical identification method, we consider (p) experimental points $[(H_i, M_i), i = 1, p]$ extracted from a given experimental first magnetization curve with a constant spacing ΔH e.g. (6) as well as their symmetrical with respect to (H, M)-plane origin [12].

$$\Delta H = H_{i+1} - H_i. \quad (6)$$

The magnetization is given as a function of temperature by:

$$M_i^T = \theta(T) \cdot M_i, \quad i = 1, p. \quad (7)$$

We create (p^2) “created points” noted (H_{ij}^*, M_{ij}^{*T}) which we arrange in the (H, M) -plane by considering:

$$\begin{cases} -H_s < H_{ij}^* < +H_s \\ -M_s^T < M_{ij}^{*T} < M_{fmc}^T(H) \end{cases} \quad (8)$$

$M_{fmc}^T(H)$ is the experimental first magnetization curve affected by temperature T , e.g. (7), and its symmetrical part with respect to the (H, M) -plane origin. H_s is the value of the excitation corresponding to the saturation magnetization M_s^T affected by temperature T .

Created points are arranged in the (H, M) -plane following the procedure [12, 13]:

a. Horizontal positioning of created points:

For a k -th experimental point (H_k, M_k^T) , we create $[(H_{kj}^*, M_{kj}^{*T}), j = 1, 2k - 1]$ points that we arrange in the (H, M) -plane limited by the lines $(H = H_k)$ and $(H = -H_k)$ with constant spacing ΔH^* , e.g. (9):

$$\begin{cases} -H_k < H_{kj}^* < +H_k \\ \Delta H^* = H_{kj+1}^* - H_{kj}^* \end{cases} \quad (9)$$

b. Vertical positioning of created points:

Magnetization value M_{kj}^{*T} is determined by considering a quantity noted δM_k^T defined below e.g. (11) and which represents the magnetization variation between two successive experimental points. Factor λ [12] enables vertical positioning of the created point (H_{kj}^*, M_{kj}^{*T}) . After arranging all points in the (H, M) -plane using (4) and considering the assumptions (i) and (ii), only $p(p + 1)$ cells in the discretized Preisach triangle are finally considered. For more precision, we develop the procedure by considering a single experimental point (Fig. 3):

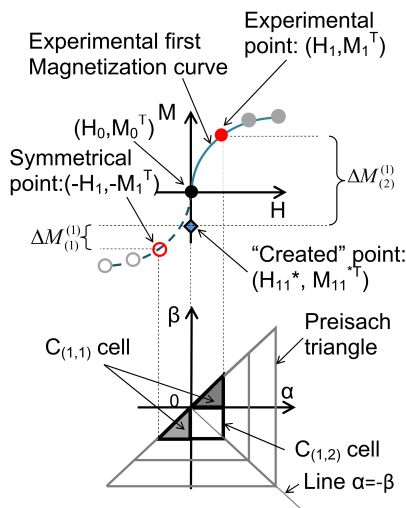


Fig. 3. An experimental curve of first magnetization and its symmetrical with respect to the origin. The single experimental point (H_1, M_1^T) considered, its symmetric $(-H_1, -M_1^T)$ and the created point (H_{11}^*, M_{11}^{*T}) in the plane (H, M)

The figure above (Fig. 3) is a schematic representation of the method for a single experimental point extracted from an experimental first magnetization curve. The scheme shows the first magnetization curve (solid line) as well as its symmetrical part with respect to the origin (dashed line). It also shows the link between the variations of the magnetization ($\Delta M_{(1)}^{(1)}$, $\Delta M_{(2)}^{(1)}$) and the construction of the Preisach discretized triangle (cells: $C_{(1,1)}$, $C_{(1,2)}$).

For one experimental point (H_1, M_1^T) and its symmetrical ($-H_1, -M_1^T$) and in order to identify the unknown content of the cell $C_{(1,1)}$, we use a created point (H_{11}^*, M_{11}^{*T}) arranged vertically and defined by (Fig. 3):

$$\begin{cases} -M_1^T < M_{11}^{*T} < M_1^T \\ H_{11}^* = 0 \end{cases} \quad (10)$$

M_{11}^{*T} is determined using the quantity δM_1^T , e.g. (11), and the factor λ which is used for the positioning of the created point (H_{11}^*, M_{11}^{*T}) with respect to the considered experimental point ($-H_1, -M_1^T$) and the origin of the plane (H, M) noted (H_0, M_0^T), (Fig. 3):

$$\begin{cases} \delta M_1^T = -M_1^T - (-M_0^T) \\ M_{11}^{*T} = M_0^T - \lambda \delta M_1^T \end{cases} \quad (11)$$

As the magnetization variation between $-M_1^T$ and M_{11}^{*T} involves only the cell $C_{(1,1)}$ (Fig. 3) and by using e.g. (4), we obtain:

$$\begin{cases} \Delta M_1^1 = M_{11}^{*T} - (-M_1^T) \\ \Delta M_1^1 = 2 \iint_{C_{(1,1)}} \nu(\alpha, \beta) d\alpha d\beta = 2\nu_{11} \end{cases} \quad (12)$$

The value of the distribution function corresponding to the cell $C_{(1,2)}$ (Fig. 3) can be determined by:

$$\begin{cases} \Delta M_2^1 = (+M_1^T) - M_{11}^{*T} \\ \Delta M_2^1 = 2 \iint_{C_{(1,1)+C_{(1,2)}}} \nu(\alpha, \beta) d\alpha d\beta = 2(\nu_{11} + \nu_{12}) \\ \Delta M_2^1 = 2\nu_{12} + \Delta M_1^1 \end{cases} \quad (13)$$

The numerical solution of the previous system of equations, e.g. (13), gives the discrete values ν_{11} and ν_{12} . With the same technique, we can generalize by considering the k -th experimental point of a cloud of p points: δM_k^T represents the magnetization variations between two successive experimental points, e.g. (14):

$$\left\{ \begin{array}{l} \delta M_k^T = -M_k^T - (-M_{k-1}^T) \\ M_{k1}^{*T} = -M_{k-1}^T - \lambda \delta M_{k-1}^T \\ M_{k2}^{*T} = -M_{k-1j}^{*T} - \lambda \delta M_{k-1}^T \\ M_{k3}^{*T} = -M_{k-1j}^{*T} - \lambda \delta M_{k-1}^T \quad j = 1: 2k-3 . \\ \dots\dots\dots \\ M_{k2k-2}^{*T} = -M_{k-1j}^{*T} - \lambda \delta M_{k-1}^T \\ M_{k2k-1}^{*T} = +M_{k-1}^T - \lambda \delta M_{k-1}^T \end{array} \right. \quad (14)$$

Using e.g. (4), we obtain an algebraic system of equations e.g. (15) whose unknowns are the discrete values of the density function v_{ij} :

$$\left\{ \begin{array}{l} \Delta M_{(1)}^{(k)} = M_{k1}^{*T} - (-M_k^T) = 2v_{kk} \\ \Delta M_{(2)}^{(k)} = M_{k2}^{*T} - M_{k1}^{*T} = 2v_{kk+1} + \Delta M_{(1)}^{(k-1)} \\ \Delta M_{(3)}^{(k)} = M_{k3}^{*T} - M_{k2}^{*T} = 2v_{kk+2} + \Delta M_{(2)}^{(k-1)} \\ \dots\dots\dots \\ \Delta M_{(2-1)}^{(k)} = M_{kj}^{*T} - M_{kj-1}^{*T} = 2v_{kh-1} + \Delta M_{(k+1)}^{(k-1)} \quad j = 1: 2k-3, \quad h = k: 3k-1 \\ \Delta M_{(2k)}^{(k)} = (M_k^T) - M_{3j}^{*T} = 2v_{kh} + 2 \sum_{n=3}^{3k-2} v_{kn} \end{array} \right. \quad (15)$$

It should be noted that for (p) experimental points, we obtain a system of $p(p+1)$ algebraic equations and $p(2p+1)$ cells of the discretized Preisach triangle.

4. Numerical results

We validated our numerical method by comparing experimental hysteresis cycles at various temperatures [18, 19] with others obtained numerically.

The figures above (Fig. 4(a) and Fig. 4(b)) show comparisons between simulated and experimental hysteresis cycles for ferromagnetic materials 3F45 [18] and Permalloy FeNi 78% [19] at different temperatures.

In the figure (Fig. 4(a)) which shows the variation of the hysteresis cycle with increasing temperature for 3F45 ferrite, the sudden drop in the coercive field is explained by:

3F45 ferrite has a low coercive field and a low Curie temperature, at temperature values close to the Curie temperature (300°C), the material tends to lose its magnetic properties rapidly in a small temperature range. This explains the sudden drop in the coercive field observed in the representation (Fig. 4(a)). In addition, a significant decrease of the saturation induction field is also observed. This phenomenon continues until the curve flattens out completely and the coercive field disappears. These remarks are in perfect agreement with the experimental observations.

Permalloy 78 (FeNi 78%) (Fig. 4(b)) has a very high permeability and a Curie temperature (between 360°C and 460°C). These characteristics mean that Permalloy 78 takes a long time to

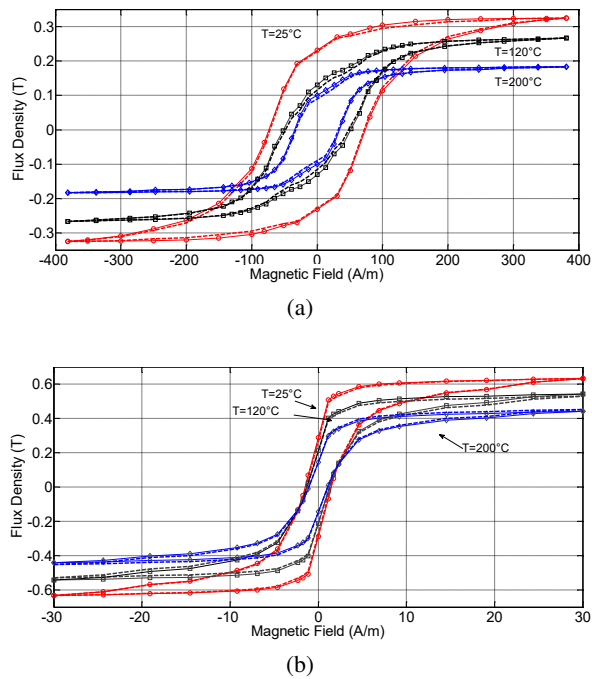


Fig. 4. Hysteresis cycles at different temperatures. Full lines with markers – measured values, dotted lines – simulated values generated by the proposed method: 3F45 ferromagnetic material (a); FeNi 78% ferromagnetic material (b)

lose its magnetization, which explains why the coercive field decreases but very slowly. In the literature [18], loss of 0.01 (A/m) per 100°C [18]. Also, it is observed that the hysteresis cycles tend to “redress” with the increasing of temperature. The coercive field as well as the saturation magnetization slowly decreases with increasing temperature.

The Figures below show the numerical Preisach distribution functions obtained for the 3F45 material (Fig. 5 and Fig. 6) and FeNi 78% material (Fig. 7 and Fig. 8) at temperatures 25°C, 120°C and 200°C.

It can be observed that the intensity of the distribution function decreases significantly with the increase of temperature. For 3F45 material (Fig. 5 and Fig. 6), this intensity decreases from the value 0.07 to the value 0.04 and for FeNi 78% (Fig. 7 and Fig. 8) it decreases from value 0.2 to value 0.12.

As the Curie temperature is approached, the Preisach distribution functions begin to disappear with the magnetic properties of the material and the hysteresis cycles become flatter.

Subsequently, the developed method was used to characterize the influence of temperature on hysterical behavior of selected ferromagnetic materials at different temperatures. The materials considered are FeSiHiB (GO) ($T_c = 750^\circ\text{C}$), FeSi 6.5% ($T_c = 690^\circ\text{C}$) and FeSi NO ($T_c = 735^\circ\text{C}$). Their magnetic properties were taken from [17, 20]. We have chosen these three iron-silicon alloys because they belong to the same class. The grain structures vary due to the different manu-

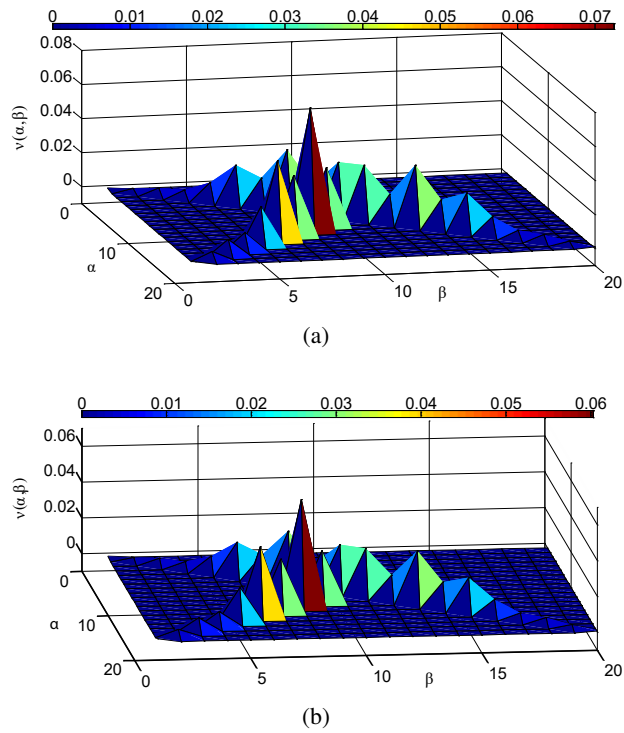


Fig. 5. Numerical Preisach distribution function generated by the numerical method for 3F45 [18] material: at 25°C (a); at 120°C (b)

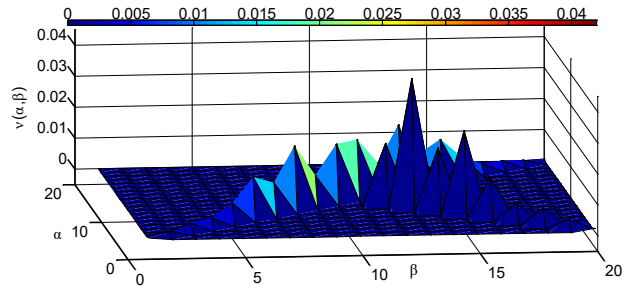
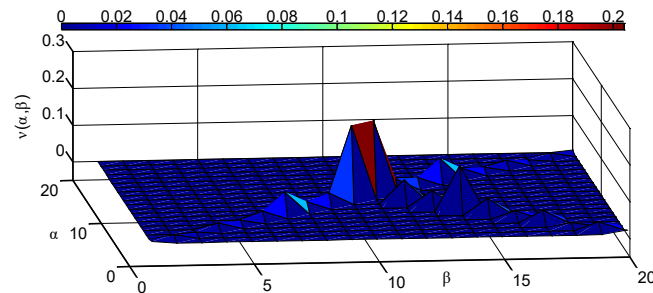
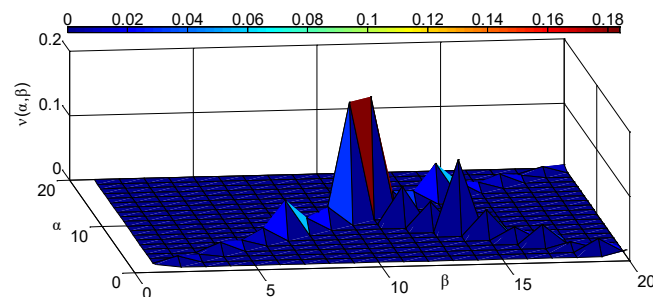


Fig. 6. Numerical Preisach distribution function generated by the numerical method for 3F45 [18] material at 200°C

facturing processes and the heat treatments. Non-grain oriented (NO) FeSi sheets are produced by hot rolling and cold rolling followed by annealing. Grain oriented (GO) sheets are hot rolled once and cold rolled twice and annealed. They have a well-known Goss texture which privileges the rolling direction as the axis of easy magnetization. The NO sheets are substantially isotropic in the plane, and the GO sheets are anisotropic in the rolling axis. The assumption of isotropy is reasonable for both FeSi 6.5% and FeSi GO materials and it is less so for FeSi NO material.



(a)



(b)

Fig. 7. Numerical Preisach distribution function generated by the numerical method for FeNi 78% [19] material: at 25°C (a); at 120°C (b)

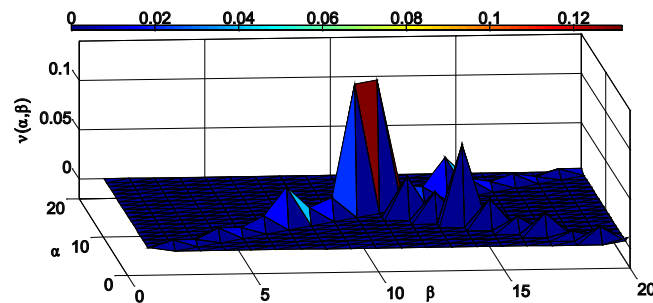


Fig. 8. Numerical Preisach distribution function generated by the numerical method for FeNi 78% [19] material at 200°C

The above curves (Fig. 9(a) and Fig. 9(b)) show the effect of temperature on the hysteresis cycles of materials FeSiHiB and FeSi 6.5%. It can be seen that the initial shape of these cycles is relatively straight, indicating that these materials have a high permeability. As the temperature increases, the induction and coercive field gradually decrease and disappear as the Curie temperature is reached.

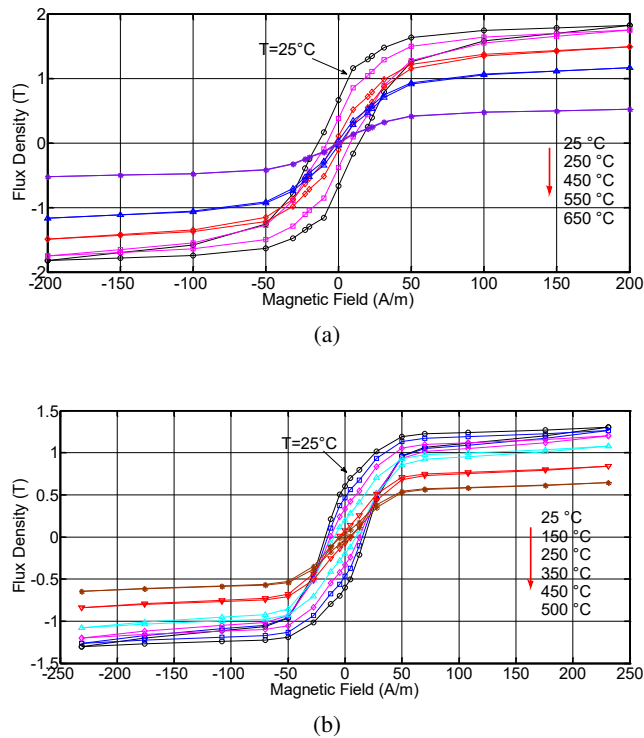


Fig. 9. Variation of simulated hysteresis cycle with temperature: FeSiHiB material (a); FeSi 6.5% material (b)

The curve (Fig. 10) shows a very meaningful decrease in the induction of saturation and in the coercive field with temperature increase. Hysteresis losses are affected because they are proportional to the cycle area. All these observations are in agreement with results published in the specialized literature. Overall, numerical simulations reproduce perfectly all the physical phenomena experimentally observed and related to magnetic hysteresis.

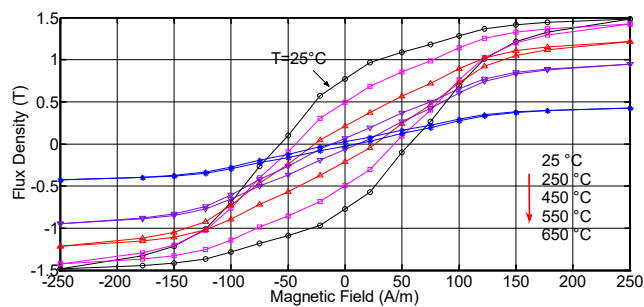


Fig. 10. Variation of simulated hysteresis cycle with temperature for material FeSi NO

5. Conclusions

In this work, we present a numerical method for identifying the Preisach distribution function by considering the effect of temperature and using a self-developed numerical method. The proposed approach is of the macroscopic phenomenological type: relationship between the variation of magnetization and the observed global hysteretic behavior. The study focuses on isotropic ferromagnetic materials, but it has the potential to be extended to other types of magnetic materials with anisotropy considerations in the future. The implementation of the developed method requires only a few experimental data points extracted from the first magnetization curve provided by metallurgists. It's a robust tool for simulating hysteresis including the effect of temperature and is intended for use by electrical equipment designers.

References

- [1] Chwastek K., *Higher order reversal curves in some hysteresis models*, Archives of Electrical Engineering, vol. 61, no. 4, pp. 455–470 (2012), DOI: [10.2478/V10171-012-0036-9](https://doi.org/10.2478/V10171-012-0036-9).
- [2] Szewczyk R., *The method of moments in Jiles–Atherton model based magnetostatic modelling of thin layers*, Archives of Electrical Engineering, vol. 67, no. 1, pp. 27–35 (2018), DOI: [10.24425/118989](https://doi.org/10.24425/118989).
- [3] Raghunathan A., Melikhov Y., Snyder J.E., Jiles D.C., *Theoretical Model of Temperature Dependence of Hysteresis Based on Mean Field Theory*, IEEE Transactions on Magnetics, vol. 46, no. 6, pp. 1507–1510 (2010), DOI: [10.1109/TMAG.2010.2045351](https://doi.org/10.1109/TMAG.2010.2045351).
- [4] Preisach F., *Über die magnetische Nachwirkung*, Zeitschrift für Physik, vol. 94, pp. 277–302 (1935), DOI: [10.1007/BF01349418](https://doi.org/10.1007/BF01349418).
- [5] Sutor A., Rupitsch S.J., Bi N., Lerch R., *A modified Preisach hysteresis operator for the modeling of temperature dependent magnetic material behavior*, Journal of Applied Physics, vol. 109, no. 7, pp. 1–4 (2011), DOI: [10.1063/1.3562520](https://doi.org/10.1063/1.3562520).
- [6] Bavendiek G., Leuning N., Müller F., Schauerte B., Thul A., Hameyer K., *Magnetic anisotropy under arbitrary excitation in finite element models*, Archives of Electrical Engineering, vol. 68, no. 2, pp. 455–466 (2019), DOI: [10.24425/ae.2019.128280](https://doi.org/10.24425/ae.2019.128280).
- [7] Sixdenier F., Scorretti R., *Numerical model of static hysteresis taking into account temperature*, International Journal of Numerical Modelling: Electronic Networks, Devices and Fields, vol. 68, no. 2, pp. 1–9 (2017), DOI: [10.1002/jnm.2221](https://doi.org/10.1002/jnm.2221).
- [8] Chen H., Xu Q., Xiang Y., Huang Y., *Temperature characteristics modeling of Preisach theory*, MATEC Web of Conferences 139 (2017), DOI: [10.1051/mateconf/201713900077](https://doi.org/10.1051/mateconf/201713900077).
- [9] Ould Ouali S.H., Mohellebi H., Chaïbi R., Féliachi M., *Introduction de l'effet de la température dans le modèle de Preisach pour la génération des cycles d'hystérésis*, Journal de Physique IV France, vol. 124, pp. 315–320 (2005), DOI: [10.1051/jp4:2005124046](https://doi.org/10.1051/jp4:2005124046).
- [10] Mayergoyz I., *Mathematical Models of Hysteresis*, IEEE Transactions on Magnetics, vol. 22, no. 5, pp. 603–608 (1986), DOI: [10.1109/TMAG.1986.1064347](https://doi.org/10.1109/TMAG.1986.1064347).
- [11] Cardelli E., Fiorucci L., Della Torre E., *Identification of the Preisach probability functions for soft magnetic materials*, IEEE Transactions on Magnetics, vol. 37, no. 5, pp. 3366–3369 (2001), DOI: [10.1109/20.952615](https://doi.org/10.1109/20.952615).
- [12] Chelghoum L., Louai F.Z., Nait-said N., *A New Approach for Preisach Distribution Function Identification Using Few Experimental Data*, Acta Electrotechnica et Informatica, vol. 14, no. 3, pp. 54–60 (2014), DOI: [10.15546/aeci-2014-0030](https://doi.org/10.15546/aeci-2014-0030).

- [13] Chelghoum L., *Étude des non Linéarités dans les Dispositifs Électriques par la Méthode de Galerkin sans maillages*, Doctoral thesis, Faculty of Technology, Batna 2 University, Algeria (2016).
- [14] Lu H.Y., Zhu J.G., Ron Hui S.Y., *Measurement and Modeling of Thermal Effects on Magnetic Hysteresis of Soft Ferrites*, IEEE Transactions on Magnetics, vol. 43, no. 11, pp. 3952–3960 (2007), DOI: [10.1109/TMAG.2007.904942](https://doi.org/10.1109/TMAG.2007.904942).
- [15] Zegadi L., Rousseau J.J., Allard B., Tenant P., Renault D., *Model of power soft MnZn ferrites, including temperature effects*, IEEE Transactions on Magnetics, vol. 36, no. 4, pp. 2022–2032 (2000), DOI: [10.1109/20.875308](https://doi.org/10.1109/20.875308).
- [16] Ladjimi A., Mékideche M.R., Babouri A., *Thermal effects on magnetic hysteresis modeling*, Archives of Electrical Engineering, vol. 61, no. 1, pp. 77–84 (2012), DOI: [10.2478/v10171-012-0007-1](https://doi.org/10.2478/v10171-012-0007-1).
- [17] <https://hal.archives-ouvertes.fr/cel-01096612>, accessed December 2014.
- [18] Chailloux T.M., *Caractérisation et modélisation de matériaux magnétiques en hautes températures en vue d'une application au filtrage CEM*, Doctoral thesis, Université Claude Bernard Lyon 1, France (2011).
- [19] Sixdenier F., Raulet M.A., Martin C., Morel L., Chailloux T., Messal O., Hilal A., *Caractérisation et modélisation de matériaux et composants magnétiques sous contrainte thermique*, Symposium de Génie Électrique (SGE'14): ef-epf-mge 2014, Cachan, France, pp. 1–9 (2014).
- [20] Fiorillo F., *Characterization and Measurement of Magnetic Materials*, Academic Press (2004).